Low-Bias Control of AMB Subject to Voltage Saturation: State-Feedback and Observer Designs

Panagiotis Tsiotras, *Senior Member, IEEE,* and Murat Arcak *Member, IEEE*

***Abstract*— This paper addresses the problem of low-bias control for an active magnetic bearing (AMB) subject to voltage saturation. Using a generalized complementarity flux condition, a simple, three-dimensional flux-based model is used to describe the dynamics of the low-bias mode of operation. Several stabilizing controllers are derived by applying recent results from nonlinear control theory. Specifically, the asymptotic small-gain theorem of Teel and passivity-based ideas are instrumental in our designs. Both soft and hard saturation constraints are accommodated. When flux measurements are not available, a nonlinear reduced-order observer is proposed to estimate the flux. We show global asymptotic stability for all controller-observer interconnections. Numerical simulations against a high fidelity AMB model show the effectiveness of the proposed control designs.**

I. Introduction

It is envisioned that future commercial and military spacecraft will have an unprecedented degree of autonomy made possible by increased on-board processing speed and memory capabilities. This increase in on-board processing, autonomous sensing and communication capabilities translates directly to large requirements for on-board available power. Traditional chemical batteries have several limitations stemming from their inherent unreliability, low depth of discharge, heavy weight, limited life, etc. A discussion on the future trends of satellite architectures and their impact on power generation and storage requirements can be found in [21], [5], [26].

An alternative to the chemical batteries for energy storage and power generation for future spacecraft has been proposed in recent years, namely, that of electromechanical (e.g., flywheel) batteries [3], [4], [9], [21], [23]. Taking into consideration that most orbiting spacecraft already incorporate spinning wheels (e.g., momentum wheels, CMG's) for attitude control, the prospect of using these wheels to also store energy seems natural and appealing. Several technical challenges need to be overcome, however, before flywheels become a part of a standard spacecraft power subsystem. One such major challenge is the design of flywheels supported on low-loss active magnetic bearings (AMB's).

Efficient operation of flywheel electromechanical batteries necessitates minimization of energy losses (mechanical and other). To avoid excessive friction losses, it is imperative to use AMB's in order to support the spinning rotor. Although mechanical (friction) losses are eliminated using AMB's, electromagnetic losses still exist in a flywheel/AMB system due to eddy current or ohmic effects. These losses can be a significant portion of the overall power losses in high-speed flywheels [1]. One way to reduce eddy current and ohmic losses is to reduce or eliminate the bias current during AMB operation [10], [12]. Owing to the nonlinear flux/force characteristic, a bias flux (or current) is typically used to linearize the AMB equations followed by a subsequent use of linear design techniques. Reduction or elimination of the bias current leads to a nonlinear region which is dominated, among other things, by slew-rate force limitations close to the origin [7]. These limitations manifest themselves as saturation constraints on the power amplifier voltage driving the coils of the electromagnets. The problem of designing low-bias control laws for AMB's subject to saturation constraints is a thus a nontrivial nonlinear control problem.

In this paper we use recent results from the theory of saturating control to design stabilizing control laws for AMBs in low-bias operation, subject to voltage saturation constraints. The main design tools in this framework are passivity [24], and the asymptotic small-gain theorem and the nested saturation designs due to Teel [29], [28]. We present three low-bias designs for an AMB. The first two designs ensure global asymptotic stability in case of soft saturation constraints. The third design ensures global asymptotic stability in case of hard

This work was supported in part by AFRL and AFOSR under Award No. F49620-00-1-0374.

P. Tsiotras is with the School of Aerospace Engineering, Georgia Institute of Technology, Atlanta, GA 30332-0150, USA (e-mail: p.tsiotras@ae.gatech.edu).

M. Arcak is with the Department of Electrical, Computer and Systems Engineering, Rensselaer Polytechnic Institute, Troy, New York, 12180-3590, USA (e-mail: arcak@ecse.rpi.edu).

voltage saturation constraints.

All controllers proposed in this work require flux feedback. Since flux may not be easily measurable in practice, a nonlinear observer is designed and incorporated in certainty-equivalence implementations of the state-feedback control laws. The stability proof of this certainty-equivalence scheme is given for each of the three control laws. Numerical examples against a high-fidelity AMB plant are used to demonstrate the theoretical developments. This AMB plant includes all effects which are neglected in the control design process: coil resistance, flux leakage, and neglected flexible dynamics. The numerical simulations show that the proposed controllers are robust against these effects.

II. Modeling of an AMB in Low Bias Mode

The simplified AMB model used in this paper consists of two identical electromagnets, which are used to move a rotor of mass m in one dimension. To regulate the position q of the mass to zero, the control designer uses the voltage inputs of the electromagnets, V_1 and V_2, in order to exert attractive forces on the rotor; see Fig. 1. Neglecting gravity, the total force generated by each

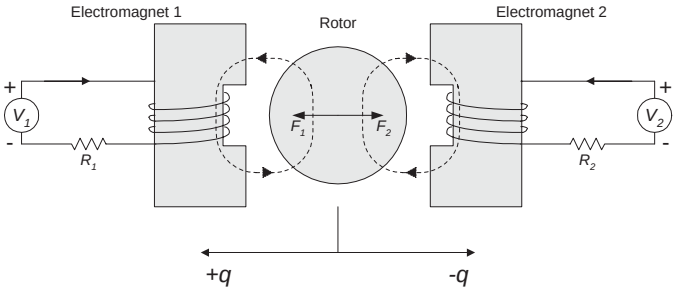

Fig. 1. Simplified one-dimensional AMB geometry.

electromagnet is given by [22],

$$F_i = \frac{\Phi_i^2}{\mu_o A_g}, \qquad i = 1, 2 \tag{1}$$

where Φ_i is the total magnetic flux of the i-th electromagnet, A_g is the cross sectional area of the airgap at the pole, and μ_o is the permeability of free space ($= 1.25 \times 10^{-6}$ H/m). In non-zero bias operation we distinguish the total magnetic flux into the bias flux Φ_0 and the perturbation (control) flux ϕ_i generated by the i-th electromagnet. The total flux generated by the i-th electromagnet is therefore,

$$\Phi_i = \Phi_0 + \phi_i, \qquad i = 1, 2. \tag{2}$$

The equation of motion of the rotor can be written as

$$\begin{aligned} \ddot{q} &= \frac{1}{\kappa}(\Phi_1^2 - \Phi_2^2) \\ &= \frac{1}{\kappa}\left[\phi_1^2 - \phi_2^2 + 2\Phi_o(\phi_1 - \phi_2)\right] \end{aligned} \tag{3}$$

where $\kappa = m\mu_o A_g$. The electrical dynamics are given by

$$\dot{\Phi}_i = \dot{\phi}_i = \frac{V_i}{N}, \qquad i = 1, 2 \tag{4}$$

where N is the number of turns of the coil of each electromagnet and V_i is the total voltage applied to each electromagnet. In (4) the coil resistance has been neglected for simplicity. This implies that a precompensator has been used to cancel the coil resistance term[1].

Let us now define the *auxiliary control flux* signal

$$\phi := \phi_1 - \phi_2 \tag{5}$$

and introduce the following flux-dependent, voltage switching scheme

$$V_1 = V, \quad V_2 = 0 \qquad \text{when} \quad \phi \geq 0, \tag{6a}$$

$$V_2 = -V, \quad V_1 = 0 \qquad \text{when} \quad \phi < 0, \tag{6b}$$

where v is a *generalized control voltage* such that

$$\dot{\phi} = \frac{V}{N}. \tag{7}$$

It can be shown [31] that under the switching strategy (6) equation (3) takes the form

$$\ddot{q} = \frac{1}{\kappa}(2\bar{\Phi}_0\phi + \phi|\phi|) \tag{8}$$

where $\bar{\Phi}_0 := \Phi_0 + \min\{\phi_1(0), \phi_2(0)\}$.

Define now the non-dimensionalized state and control variables

$$\begin{gathered} x_1 = \frac{q}{g_0}, \quad x_2 = \frac{\dot{q}}{\Phi_{\text{sat}}\sqrt{g_0/\kappa}}, \quad x_3 = \frac{\phi}{\Phi_{\text{sat}}}, \\ v = \frac{V\sqrt{g_0\kappa}}{N\Phi_{\text{sat}}^2}, \end{gathered} \tag{9}$$

along with the non-dimensionalized time

$$\tau = t\frac{\Phi_{\text{sat}}}{\sqrt{g_0\kappa}},$$

where g_0 is the nominal air-gap and Φ_{sat} is the value of the saturation (maximum) flux. Then one obtains the following non-dimensionalized system in state-space form

$$x_1' = x_2 \tag{10a}$$

$$x_2' = \varepsilon x_3 + x_3|x_3| \tag{10b}$$

$$x_3' = v \tag{10c}$$

[1]Depending on the resistance variation with temperature, this may not be necessary. Modern PWM power amplifiers (e.g., Copley Controls 412) when operated in voltage mode, automatically compensate for the voltage drop across the (constant) coil resistance. For the effect of the neglected coil resistance in equation (4) see also Section VIII.

where $\varepsilon = 2\bar{\Phi}_0/\Phi_{\rm sat}$ $(0 \leq \varepsilon \ll 1)$ and where prime denotes differentiation with respect to the new independent variable τ. Notice that for $\varepsilon = 0$ this model reduces to the zero bias case[2]. Zero-bias control design for AMBs is especially challenging because of the loss of linear controllability when $\varepsilon = 0$. References [30], [31] present a complete analysis of the zero-bias AMB control problem. Note that although by definition $|x_3| \leq 1$, this constraint will not be taken into consideration in the sequel.

In this paper we are primarily interested in the case when the maximum absolute value of v is limited due to voltage saturation. If, for instance, it is known that $|V| \leq V_{\max}$ then (10c) must be replaced with

$$x_3' = \mathrm{sat}_\lambda(v) := \mathrm{sgn}(v)\min\{\lambda, |v|\} \tag{11}$$

where $\lambda = V_{\max}\sqrt{g_0\kappa}/N\Phi_{\rm sat}^2$. For notational simplicity, henceforth we use a dot to denote differentiation with respect to τ. Also, we will let $x := (x_1, x_2, x_3)^T \in \mathbb{R}^3$.

Notice that the voltage switching strategy (6) is such that $\min\{\phi_1, \phi_2\}$ stays constant along trajectories. As a result, any control law that renders the closed-loop system (10) globally asymptotically stable will also ensure boundedness of ϕ_1 and ϕ_2 and, in addition, that $\lim_{t\to\infty}\phi_1(t) = \lim_{t\to\infty}\phi_2(t) = \min\{\phi_1(0), \phi_2(0)\}$; see [31] for the details.

III. Low-bias vs. Zero-bias AMB Operation

The main reason for low-bias operation is reduction of power losses. The motivation behind the flux-based voltage switching scheme (6) is that under the generic assumption that $\phi_1(0) = \phi_2(0) = 0$ we have the following *generalized complementary flux condition* (gcfc) on the *perturbation* flux ϕ_i [30], [31]

$$\begin{aligned} \phi_1 = \phi, \quad \phi_2 = 0 \quad \text{when} \quad \phi \geq 0, \\ -\phi_2 = \phi, \quad \phi_1 = 0 \quad \text{when} \quad \phi \leq 0. \end{aligned} \tag{12}$$

This constraint ensures that only one control force acts on each electromagnet at a time, thus avoiding unnecessary competition between the two electromagnets. Moreover, the gcfc operation constraint tends to reduce the overall flux, thus ensuring smaller power losses.

It should be pointed out that the gcfc is somewhat different than the classical *complementary flux condition* (cfc) used for zero-bias operation ($\Phi_0 = 0$)

$$\begin{aligned} \Phi = \quad \Phi_1, \quad \Phi_2 = 0 \quad \text{when} \quad \Phi \geq 0, \\ \Phi = -\Phi_2, \quad \Phi_1 = 0 \quad \text{when} \quad \Phi < 0, \end{aligned} \tag{13}$$

[2]The initial control fluxes $\phi_1(0)$ and $\phi_2(0)$ are typically small and can be taken without loss of generality (or by the definition of Φ_0) to be zero. Even if this is not the case, these are spurious fluxes which shall dissipate very quickly due to coil resistance or by the bias-setting control law; see [31].

in the sense that the gcfc is imposed on the *perturbation* flux rather than on the total flux. When the bias flux is taken to be zero ($\Phi_0 = 0$) however, the gcfc scheme reduces to the standard AMB model operating at cfc mode (13). Moreover, the gcfc scheme ensures controllability of the resulting system as $\Phi_0 \to 0$. This is not the case when using, say, the normal or constant sum flux biasing scheme [31], [15].

As already mentioned, small bias is used in order to reduce ohmic and eddy current losses. In the limiting case $\Phi_0 \to 0$, one could eliminate the bias completely and (along with the standard cfc) achieve a great reduction in power losses [7]. However, zero-bias operation imposes severe limitations on the AMB operation. Notice

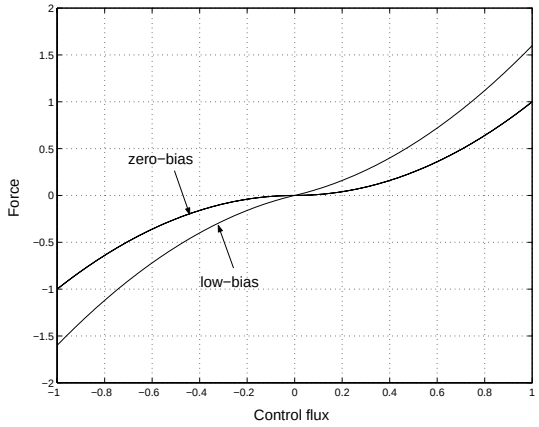

Fig. 2. Zero-bias and Low-bias characteristics.

from (8) that for zero-bias operation ($\Phi_0 = 0$), the total force exerted on the rotor is given by

$$\ddot{q} = \frac{1}{\kappa}\,\phi\,|\phi| = \frac{1}{\kappa}\,\Phi\,|\Phi|\,. \tag{14}$$

The difficulties arising from the zero-bias operation become apparent when looking at the plot of applied flux vs. total generated force for each mode, shown in Fig. 2. From this figure it is seen that for the zero-bias case the slope of the force vs. flux curve near the origin is zero. This implies that in order to produce a small control force we need a large *change* in flux resulting in large voltage commands and potential voltage saturation. In other words, for zero-bias operation, we have a situation resembling a "dead zone" near the origin. This problem is well-known in the AMB literature and it is the main reason for introducing a flux (or current) bias. As the bias flux increases, the slope at the origin gets steeper, leading to better dynamic response of the AMB [19]. This, however, is achieved at the price of higher power losses. A compromise is needed between dynamic response and power losses due to the bias fluxes. This compromise

has motivated the low-bias control designs presented in this paper. We emphasize that, while low-bias control may not be a very difficult control problem (at least for local/linearized designs), the low-bias control problem *with voltage saturation* is challenging.

IV. Passivation Design

In this section we develop a passivation design to stabilize the low-bias AMB system

$$\dot{x}_1 = x_2 \tag{15a}$$
$$\dot{x}_2 = \varepsilon x_3 + x_3|x_3| := \varepsilon x_3 + \eta(x_3) \tag{15b}$$
$$\dot{x}_3 = v\,. \tag{15c}$$

Our design starts with the preliminary feedback

$$v = -k_2 x_2 - k_3 x_3 + u\,, \quad k_2,\, k_3 > 0. \tag{16}$$

As shown below this feedback law (with $u = 0$) renders the equilibrium $x = 0$ stable with a Lyapunov function V satisfying $\dot{V} \leq 0$. Asymptotic stability is then achieved by applying a saturated $L_g V$-type control law as in Sepulchre *et al.* [24]. To compute such a V we introduce the new variable

$$\zeta := k_2 x_1 + (k_3/\varepsilon) x_2 + x_3\,, \tag{17}$$

and rewrite the system (15)-(16) as

$$\dot{\zeta} = \frac{k_3}{\varepsilon} x_3|x_3| + u \tag{18a}$$
$$\dot{x}_2 = \varepsilon x_3 + x_3|x_3| \tag{18b}$$
$$\dot{x}_3 = -k_2 x_2 - k_3 x_3 + u\,. \tag{18c}$$

Then the choice

$$V(\zeta, x_2, x_3) = \frac{\varepsilon^2}{k_1}\int_0^{k_1\zeta} \mathrm{sat}(s)\,\mathrm{d}s + \frac{k_2}{2}x_2^2 + \frac{\varepsilon}{2}x_3^2 + \frac{1}{3}|x_3|x_3^2 \tag{19}$$

satisfies

$$\begin{aligned}\dot{V} &= \varepsilon^2 \mathrm{sat}(k_1 z)\frac{k_3}{\varepsilon}|x_3|x_3 + k_2 x_2(\varepsilon x_3 + |x_3|x_3) \\ &\quad -\varepsilon\, x_3(k_2 x_2 + k_3 x_3) - x_3|x_3|(k_2 x_2 + k_3 x_3) \\ &\quad +(\varepsilon^2 \mathrm{sat}(k_1\zeta) + \varepsilon x_3 + x_3|x_3|)u \\ &= \varepsilon\,\mathrm{sat}(k_1\zeta) k_3 x_3|x_3| - \varepsilon k_3 x_3^2 - k_3 x_3^2|x_3| \\ &\quad +(\varepsilon^2 \mathrm{sat}(k_1\zeta) + \varepsilon x_3 + x_3|x_3|)u \\ &\leq -k_3 x_3^2|x_3| + (\varepsilon^2 \mathrm{sat}(k_1\zeta) + \varepsilon x_3 + x_3|x_3|)u \end{aligned} \tag{20}$$

which means that the system (18) with input u and output $y = \varepsilon^2 \mathrm{sat}(k_1\zeta) + \varepsilon x_3 + x_3|x_3|$ is passive. With $u = 0$, the origin $x = 0$ is stable but not asymptotically stable, because the system (18) has a continuum of equilibria at $(\zeta_0, 0, 0)$, $\zeta_0 \in \mathbb{R}$. To increase the negativity in (20) we apply the feedback

$$u = -\mathrm{sat}_\lambda(y) = -\mathrm{sat}_\lambda(\varepsilon^2 \mathrm{sat}(k_1\zeta) + \varepsilon x_3 + x_3|x_3|) \tag{21}$$

which ensures global asymptotic stability for any saturation level $\lambda > 0$. This is shown in the next theorem.

Theorem 1: Consider the system (15), and let the variable ζ be as in (17). Then, the control law

$$\boxed{v = -k_2 x_2 - k_3 x_3 - \mathrm{sat}_\lambda(\varepsilon^2 \mathrm{sat}(k_1\zeta) + \varepsilon x_3 + x_3|x_3|)} \tag{22}$$

where $k_1, k_2, k_3, \lambda > 0$, globally asymptotically stabilizes the origin $x = 0$.

Proof: From (20) and (21), it follows that the set in which $\dot{V} = 0$ is $E = \{(\zeta, x_2, x_3) : \zeta = x_3 = 0\}$. When $x_3 \equiv 0$ and $\zeta \equiv 0$ then $u \equiv 0$ and thus $\dot{x}_3 \equiv 0$ which along with $x_3 = u = 0$ implies via (18c) that $x_2 = 0$. Therefore the largest invariant set in E is the equilibrium $x = 0$. Asymptotic stability follows from LaSalle's invariance principle. ∎

V. Small Gain Design

Our next design makes use of an asymptotic small gain theorem by Teel [29]. Before presenting the main result from [29] used herein, we let $|y| := \max_i |y_i|$ denote the norm for a vector $y \in \mathbb{R}^n$, and for a signal $y(t)$, we denote

$$\|y\|_a = \lim_{t\to\infty} \sup |y(t)|\,. \tag{23}$$

The following result, adapted from [29, Theorem 3], is instrumental in our design:

Proposition 1: Consider the system

$$\dot{x} = Ax + Bu + w \tag{24a}$$
$$\dot{z} = f(z, u, d) \tag{24b}$$
$$w = g(z, u, d) \tag{24c}$$

where $x \in \mathbb{R}^{n_1}$, $z \in \mathbb{R}^{n_2}$, A is marginally stable; that is, there exists a matrix $P = P^T > 0$ satisfying

$$A^T P + PA \leq 0\,, \tag{25}$$

the function $f(z, u, d)$ is locally Lipschitz, and the function $g(z, u, d)$ is continuous satisfying

$$\lim_{|(z,u)|\to 0} \frac{|g(z, u, 0)|}{|(z, u)|} = 0\,. \tag{26}$$

Suppose, for the z-subsystem (24), there exists a locally Lipschitz class-$\mathcal{K}$ function $\gamma_1(\cdot)$ such that, for each bounded $u(t)$ and $d(t)$, the solution $z(t)$ exists for all $t \in [0, \infty)$, and

$$\|z\|_a \leq \gamma_1(\|u\|_a + \|d\|_a)\,. \tag{27}$$

Then, there exist positive constants Δ and λ^* such that, for each bounded $d(t)$ satisfying $\|d\|_a \leq \Delta$, and for each $\lambda \in (0, \lambda^*]$, the control law

$$u = -\mathrm{sat}_\lambda\left(B^T P x + d\right), \tag{28}$$

perturbed by d, ensures that the closed-loop solutions $(x(t), z(t))$ are bounded, and

$$\|(x,z)\|_a \leq \gamma_2(\|d\|_a) \tag{29}$$

for some class-$\mathcal{K}$ function $\gamma_2(\cdot)$. □

An advantage of the saturation design (28) is that it guarantees robustness against small measurement disturbances d. When the disturbance converges to zero, that is when $\|d\|_a = 0$, then (29) implies $\|(x,z)\|_a = 0$, which means that the trajectories $(x(t), z(t))$ converge to the origin.

We now apply this design methodology to the AMB system (15). Here we assume that there are no measurement disturbances, i.e., $d(t) \equiv 0$, and we design a globally asymptotically stabilizing control law as in (28). In Section VII we will implement this control law with state estimates obtained from an observer, and prove stability using the robustness property (29), where d is the observer error.

With the preliminary feedback (16), the (x_2, x_3)-subsystem plays the role of the z-subsystem in Proposition 1 because, as we prove in Theorem 2 below, it satisfies the gain property (27). Next, we note that the system (15)-(16) is of the form

$$\dot{x} = Ax + Bu + w \tag{30}$$

with

$$A = \begin{bmatrix} 0 & 1 & 0 \\ 0 & 0 & \varepsilon \\ 0 & -k_2 & -k_3 \end{bmatrix}, \quad B = \begin{bmatrix} 0 \\ 0 \\ 1 \end{bmatrix},$$
$$w = \begin{bmatrix} 0 \\ x_3\,|x_3| \\ 0 \end{bmatrix}.$$

The overall system decomposition is shown in Fig. 3. The design in Proposition 1 is now applicable because A is marginally stable, and $g(z,u,d)$, given by w above, satisfies (26).

Theorem 2: For the system (15), let A and B be as in (31) with design parameters $k_2, k_3 > 0$, and let $P = P^T > 0$ be such that $A^TP + PA \leq 0$. Then, there exists a constant λ^* such that, for every $\lambda \in (0, \lambda^*]$, the control law

$$\boxed{v = -k_2x_2 - k_3x_3 - \mathrm{sat}_\lambda\left(B^TPx\right)} \tag{31}$$

globally asymptotically stabilizes the equilibrium $x = 0$.

Proof: We first note that the Jacobian linearization of the closed-loop system is $\dot{x} = (A - BB^TP)x$, where $A - BB^TP$ is Hurwitz because (A, B) is controllable.

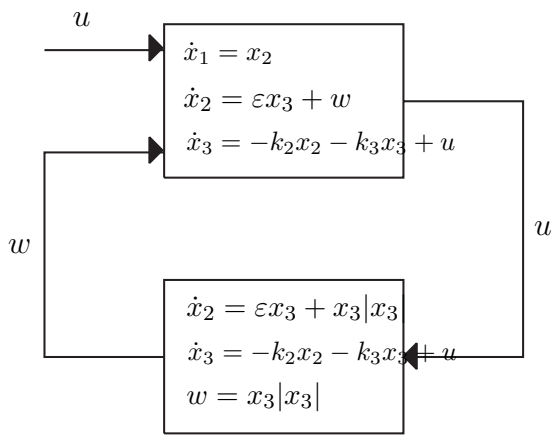

Fig. 3. System decomposition for the AMB problem.

Thus, the equilibrium $x = 0$ is locally asymptotically stable. To prove global attractivity of $x = 0$, we employ Proposition 1 and show that the z-subsystem, rewritten here as

$$\begin{aligned} \dot{x}_2 &= \varepsilon x_3 + x_3\,|x_3| \\ \dot{x}_3 &= -k_2x_2 - k_3x_3 + u\,, \end{aligned} \tag{32}$$

satisfies the gain condition (27). To this end we let

$$V = \frac{k_2}{2}x_2^2 + \frac{\varepsilon}{2}x_3^2 + \mu x_2x_3 + \frac{1}{3}|x_3|x_3^2 \tag{33}$$

where

$$0 < \mu < \min\{k_3, \sqrt{k_2\varepsilon}, \frac{4\varepsilon k_2k_3}{4\varepsilon k_2 + k_3^2}\} \tag{34}$$

It can be readily shown that V is positive definite. The derivative of V along the trajectories of (32) is

$$\begin{aligned} \dot{V} &= -\varepsilon\bar{\mu}x_3^2 - k_2\mu x_2^2 - \mu k_3x_2x_3 \\ &\quad -\bar{\mu}|x_3|x_3^2 + \varepsilon x_3u + u|x_3|x_3 + \mu x_2u \\ &\leq -a_1|x|^2 + (\varepsilon+\mu)|x||u| + |u||x_3|^2 - \bar{\mu}|x_3|^3 \end{aligned}$$

where

$$a_1 = \frac{1}{2}\left(\varepsilon\bar{\mu} + \mu k_2 - \sqrt{(\varepsilon\bar{\mu} - \mu k_2)^2 + \mu^2k_3^2}\right) > 0$$

and $\bar{\mu} = k_3 - \mu$. Using Young's inequality [14, p. 75] we have

$$|u||x_3|^2 \leq \frac{4}{27}\frac{1}{\bar{\mu}^2}|u|^3 + \bar{\mu}|x_3|^3$$

Thus,

$$\dot{V} \leq -a_1|x|^2 + a_2|x||u| + a_3|u|^3 \tag{35}$$

where $a_2 = \varepsilon + \mu$ and $a_3 = 4/27\bar{\mu}^2$. Upon completion of squares, the last inequality yields

$$\dot{V} \leq -(a_1 - \frac{a_2}{2}b)|x|^2 + \frac{a_2}{2b}|u|^2 + a_3|u|^3 \tag{36}$$

where b a positive number such that $b < 2a_1/a_2$. From (36) it follows that $\dot{V} < 0$ whenever $|x| >$

$\sqrt{c_1|u|^2+c_2|u|^3}=\rho(|u|)$ with $c_1=a_2/b(2a_1-a_2b)$ and $c_2=2a_3/(2a_1-a_2b)$. Now let $c_3=\frac{1}{4}(k_2+\varepsilon-\sqrt{(k_2-\varepsilon)^2+4\mu^2})$ and $c_4=\frac{1}{4}(k_2+\varepsilon+\sqrt{(k_2-\varepsilon)^2+4\mu^2})$ and note that

$$\underline{\alpha}(|x|)=c_3|x|^2\le V(x)\le c_4|x|^2+\frac{1}{3}|x|^3=\bar{\alpha}(|x|).$$

Using [8, Fact 37] we conclude that

$$\|(x_2,x_3)\|_a\le\gamma_1(\|u\|_a) \tag{37}$$

where $\gamma_1(s)=\underline{\alpha}^{-1}(\bar{\alpha}(\rho(s)))=\sqrt{b_1s^2+b_2s^3+(b_3s^2+b_4s^3)^{3/2}}$, $b_1=c_4c_1/c_3$, $b_2=c_4c_2/c_3$, $b_3=c_1/(3c_3)^{2/3}$, $b_4=c_2/(3c_3)^{2/3}$. Thus, from Proposition 1, the solution $x(t)$ exists for all $t\in[0,\infty)$, and $\|x\|_a=0$, that is, the equilibrium $x=0$ is globally attractive. ■

Remark 1: The feedback control B^TPx in (31) can be substituted by another feedback Fx with the matrix $A-BF$ Hurwitz. Such a matrix F can be found using the results of [27], [18].

Remark 2: The control law (31) as well as the control law (22) are saturated only partially. We call such controllers "soft saturation" controllers to distinguish them from controllers that saturate the total control signal. We shall call the latter "hard saturation" controllers; one such hard saturation controller is given next.

VI. Nested Saturation Design

The control laws (22) and (31) are only partially saturated. We now design a completely saturated control law following the *nested saturation* scheme of Teel [28], [29]. Unlike the general procedure in [28], [29], in the following proposition we explicitly compute the admissible saturation levels.

Proposition 2: Consider the system (15). The control law (38)-(39) globally asymptotically stabilizes the equilibrium $x=0$.

Proof: With $y_3:=kx_3$, $y_2:=\dfrac{k^2x_2}{\varepsilon}+kx_3$, and $y_1:=\dfrac{k^3x_1}{\varepsilon}+\dfrac{2k^2}{\varepsilon}x_2+kx_3$, and with the new independent variable $\sigma=k\tau$, the closed-loop system (15),(38), is rewritten (with an obvious abuse of notation) as

$$\dot{y}_1 = y_2+y_3+v+\frac{2}{\varepsilon}y_3|y_3| \tag{40}$$

$$\dot{y}_2 = y_3+v+\frac{1}{\epsilon}y_3|y_3| \tag{41}$$

$$\dot{y}_3 = v=-\mathrm{sat}_{\lambda_1}(y_3+v_2)\,, \tag{42}$$

where $\epsilon:=k\varepsilon$ and where $v_2=\mathrm{sat}_{\lambda_2}(y_2+\mathrm{sat}_{\lambda_3}(y_1))$. First, we note from the *feedforward* structure that the closed-loop system does not exhibit finite escape time. Next, because $|v_2|\le\lambda_2$ in (42), the Lyapunov function $V_3=\frac{1}{2}y_3^2$ satisfies $\dot{V}_3<0$ whenever $|y_3|>\lambda_2$ and, hence $\|y_3\|_a\le\lambda_2$. Using $\lambda_2<\lambda_1/2$, it follows that the saturation function $\mathrm{sat}_{\lambda_1}(y_3+v_2)$ operates in its linear region after a finite time t_1. Thus, for $t\ge t_1$,

$$v=-y_3-v_2=-y_3-\mathrm{sat}_{\lambda_2}(y_2+\mathrm{sat}_{\lambda_3}(y_1))\,, \tag{43}$$

and the y_2-subsystem is

$$\dot{y}_2=-\mathrm{sat}_{\lambda_2}(y_2+v_3)+w_2 \tag{44}$$

where $v_3=\mathrm{sat}_{\lambda_3}(y_1)$ and $w_2=\frac{1}{\epsilon}y_3|y_3|$. Using the Lyapunov function $V_2=\frac{1}{2}y_2^2$ one can show that $\dot{V}_2<0$ whenever $|w_2|<\lambda_2$ and $|y_2|>|v_3|+|w_2|$. Because $\|w_2\|_a\le\frac{1}{\epsilon}\|y_3\|_a^2\le\frac{1}{\epsilon}\lambda_2^2<\lambda_2$ from (39), it follows that $\|y_2\|_a\le\|v_3\|_a+\|w_2\|_a$. From this inequality and using $\|v_3\|_a\le\lambda_3$, $\|w_2\|_a\le\frac{1}{\epsilon}\lambda_2^2$ and the last inequality in (39), it is not difficult to show that $\|y_2\|_a+\|v_3\|_a<\lambda_2$; that is, after a finite time $t_2\ge t_1$,

$$v_2=\mathrm{sat}_{\lambda_2}(y_2+v_3)=y_2+v_3, \tag{45}$$

which implies that

$$v=-y_2-y_3-\mathrm{sat}_{\lambda_3}(y_1). \tag{46}$$

This means that, for $t\ge t_2$, the y_1-subsystem is

$$\dot{y}_1=-\mathrm{sat}_{\lambda_3}(y_1)+w_3 \tag{47}$$

where $w_3:=\frac{2}{\epsilon}y_3|y_3|$. We first note that a λ_3 satisfying the last inequality in (39) exists because $\lambda_2<\epsilon/5$ in the second inequality. Next, because $\lambda_3>2\lambda_2^2/\epsilon$, it follows from (47) that $\|y_1\|_a\le\|w_3\|_a\le\frac{2}{\epsilon}\lambda_2^2<\lambda_3$, which means that, after a finite time t_3, $\mathrm{sat}_{\lambda_3}(y_1)=y_1$. Thus, for $t\ge t_3\ge t_2$, the closed-loop system is

$$\dot{y}_1 = -y_1+\frac{2}{\epsilon}y_3|y_3| \tag{48a}$$

$$\dot{y}_2 = -y_1-y_2+\frac{1}{\epsilon}y_3|y_3| \tag{48b}$$

$$\dot{y}_3 = -y_2-y_2-y_3\,. \tag{48c}$$

We conclude the proof by showing that this system is globally asymptotically stable. Indeed, the derivative of the Lyapunov function

$$V=3y_1^2-4y_1y_2+8y_2^2+\frac{8}{3\epsilon}y_3^2|y_3| \tag{49}$$

along the trajectories of (48) is

$$\dot{V}=-2y_1^2-8y_1y_2-16y_2^2-\frac{8}{\epsilon}y_3^2|y_3|\,, \tag{50}$$

which is negative definite. Thus, the system (15), (38) is globally asymptotically stable. ■

$$\boxed{v = -\mathrm{sat}_{\lambda_1}\left(kx_3 + \mathrm{sat}_{\lambda_2}\left(\frac{k^2}{\varepsilon}x_2 + kx_3 + \mathrm{sat}_{\lambda_3}\left(\frac{k^3}{\varepsilon}x_1 + \frac{2k^2}{\varepsilon}x_2 + kx_3\right)\right)\right)} \tag{38}$$

with

$$0 < k, \quad 0 < \lambda_1, \quad 0 < \lambda_2 < \min\left\{\frac{\lambda_1}{2}, \frac{k\varepsilon}{5}\right\}, \quad \frac{2}{\varepsilon k}\lambda_2^2 < \lambda_3 < \frac{1}{2}\left(\lambda_2 - \frac{1}{\varepsilon k}\lambda_2^2\right) \tag{39}$$

VII. Flux Observer Design and Output Feedback Control

Thus far, our designs relied on the availability of flux measurements, which may be difficult in practice [11], [20]. Another approach, employed in [16], is to estimate the flux from current and position measurements using the formula

$$\Phi = \frac{\mu_0 A_g N I}{2(g_0 \pm q)}\,. \tag{51}$$

See also [20], [6]. This equation, which is essentially Ampere's law, is accurate for low frequencies but it does not account for hysteresis and eddy current effects. During transients a high frequency estimator of the flux can obtained via Faraday's law. A combination of the high-frequency and the low-frequency flux models have been used in [11] to provide an estimate of the flux without a flux sensor. This flux estimator compensates for eddy current effects, but cannot compensate for hysteresis effects and uncertainty in gaps due to thermal growth. The scheme in [11], however, still uses current measurement to estimate flux.

Another complication arises in our case due to the voltage switching scheme (6) which requires knowledge of the auxiliary signal $\phi = \phi_1 - \phi_2$. For correct implementation of the flux-based voltage switching scheme (6) it is imperative to know the *sign* of ϕ even if its exact value is not measurable or not known. During hardware implementation, the sign of ϕ can be easily inferred by a simple comparator of the coil currents of the two electromagnets. We henceforth assume that such a setup is available.

If flux or current measurements are not available, the following approach can be used to estimate the flux. Because the system nonlinearity $\eta(x_3) = x_3|x_3|$ in (15) is non-decreasing, we pursue the observer design of Arcak and Kokotović [2] for this class of nonlinearities. When ε is small as in low bias applications, a full-order design gives rise to large observer transients. We circumvent this problem with a reduced-order variant of the observer in [2]:

Proposition 3: Consider the system (15) with the output $y = x_2$, and define the new variable $\chi := x_3 - (\kappa/\varepsilon)y$ where $\kappa > 0$ is a design parameter. With the reduced-order observer

$$\dot{\hat{\chi}} = v - \kappa\,(\hat{\chi} + \frac{\kappa}{\varepsilon}\,y) - \frac{\kappa}{\varepsilon}\,\eta(\hat{\chi} + \frac{\kappa}{\varepsilon}\,y) \tag{52a}$$

$$\hat{x}_3 = \hat{\chi} + \frac{\kappa}{\varepsilon}\,y\,, \tag{52b}$$

the observer error $d(t) := \hat{x}_3(t) - x_3(t)$ satisfies, for all t in the maximal interval of existence $[0, t_f)$ of (15), (52),

$$|d(t)| \le |d(0)|e^{-\kappa t}. \tag{53}$$

Proof: Because the derivative of χ is

$$\dot{\chi} = v - \kappa x_3 - \frac{\kappa}{\varepsilon}\eta(x_3) = v - \kappa(\chi + \frac{\kappa}{\varepsilon}x_2) - \frac{\kappa}{\varepsilon}\eta(\chi + \frac{\kappa}{\varepsilon}x_2)\,, \tag{54}$$

the observation error $d = \hat{\chi} - \chi$ satisfies

$$\dot{d} = \dot{\hat{\chi}} - \dot{\chi} = -\kappa d - \frac{\kappa}{\varepsilon}\left[\eta(\hat{\chi} + \frac{\kappa}{\varepsilon}y) - \eta(\chi + \frac{\kappa}{\varepsilon}y)\right]. \tag{55}$$

Next, because the function $\eta(x_3) = x_3|x_3|$ is non-decreasing, we get

$$(\hat{\chi} - \chi)\left[\eta(\hat{\chi} + \frac{\kappa}{\varepsilon}x_2) - \eta(\chi + \frac{\kappa}{\varepsilon}x_2)\right] \ge 0\,, \tag{56}$$

from which the derivative of $V = \frac{1}{2}d^2$ satisfies

$$\dot{V} \le -\kappa d^2 = -2\kappa V\,, \tag{57}$$

thus proving (53). ■

The separation principle does not hold for general nonlinear systems; that is, a state feedback control law may be destabilizing when implemented with observer estimates. We now prove that the control laws derived in this paper preserve stability with the observer (52).

Theorem 3: Consider the system (15) and the observer (52). Either one of the control laws (22), (31), or (38), implemented with $\hat{x}_3$ instead of x_3, globally asymptotically stabilizes the origin $(x, \hat{\chi}) = 0$.

Proof: We first prove stability for the passivation design (22). When x_3 is replaced with $\hat{x}_3 = x_3 + d$, the

resulting output feedback control law $\tilde{v}$ differs from the state feedback control law v in (22), by

$$\begin{aligned}\tilde{d} := v - \tilde{v} = k_3 d + \mathrm{sat}_\lambda(\varepsilon^2 \mathrm{sat}(k_1(z+d)) + \varepsilon(x_3+d) \\ + (x_3+d)|x_3+d|) - \mathrm{sat}_\lambda(\varepsilon^2 \mathrm{sat}(k_1 z) \\ + \varepsilon x_3 + x_3|x_3|)\,.\end{aligned} \tag{58}$$

Then, the derivative of the Lyapunov function (19), along the trajectories of (15) with $\tilde{v}$, satisfies

$$\dot{V} \leq -k_3|x_3|^3 - (\varepsilon^2 \mathrm{sat}(k_1 z) + \varepsilon x_3 + x_3|x_3|)\tilde{d}\,. \tag{59}$$

Using the inequalities

$$x_3|x_3|\tilde{d} \leq \frac{k_3}{4}|x_3|^3 + \left(\frac{4}{k_3}\right)^2 |\tilde{d}|^3 \tag{60}$$

(to see this, consider the two cases $|\tilde{d}| \leq \frac{k_3}{4}|x_3|$ and $|x_3| \leq \frac{4}{k_3}|\tilde{d}|$), and

$$\varepsilon x_3 \tilde{d} \leq \frac{k_3}{4}|x_3|^3 + \varepsilon|\tilde{d}|\sqrt{\frac{4\varepsilon}{k_3}|\tilde{d}|} \tag{61}$$

(consider the two cases $|\tilde{d}| \leq \frac{k_3}{4\varepsilon}|x_3|^2$ and $|x_3| \leq \sqrt{\frac{4\varepsilon}{k_3}|\tilde{d}|}$), we obtain

$$\dot{V} \leq -\frac{k_3}{2}|x_3|^3 + \left[\varepsilon^2|\tilde{d}| + \left(\frac{4}{k_3}\right)^2 |\tilde{d}|^3 + \varepsilon|\tilde{d}|\sqrt{\frac{4\varepsilon}{k_3}|\tilde{d}|}\right]. \tag{62}$$

Next, letting T be in the maximal interval of existence $[0, t_f)$ of the closed-loop system and integrating both sides of (62) from 0 to T, we obtain

$$\begin{aligned}V(x(T)) - V(x(0)) \leq \int_0^T \left[\varepsilon^2|\tilde{d}| + \left(\frac{4}{k_3}\right)^2 |\tilde{d}|^3 \right. \\ \left. + \varepsilon|\tilde{d}|\sqrt{\frac{4\varepsilon}{k_3}|\tilde{d}|}\right] \mathrm{d}t\,.\end{aligned} \tag{63}$$

Because $\tilde{d}$ is exponentially decaying from (53) and (58), the integral on the right-hand side has an upper-bound which is independent of T. This proves that $t_f = \infty$, and the trajectories are bounded. Finally, because d converges to zero, it follows from LaSalle's invariance principle that the solutions converge to the largest invariant set where $d = 0$. When $d = 0$, the output feedback control law coincides with the state feedback control law and, hence, the largest invariant set is the origin. This concludes the proof of global asymptotic stability for the passivation design (22).

When the small gain design (31) is implemented with $\hat{x}_3$, the closed-loop system is

$$\begin{aligned}\dot{x}_1 &= x_2 \\ \dot{x}_2 &= \varepsilon x_3 + x_3|x_3| \\ \dot{x}_3 &= -k_2 x_2 - k_3(x_3+d) - \mathrm{sat}_\lambda(B^T P \hat{x})\end{aligned} \tag{64}$$

where $\hat{x} := (x_1\ x_2\ \hat{x}_3)^T$. To show that there is no finite escape time, we assume $t_f < \infty$ and let $T \in [0, t_f)$. The arguments used in the proof of Theorem 2 show that the (x_2, x_3) subsystem is *input-to-state stable* [25, Lemma 2.14] with respect to the disturbance $\tilde{u} = -k_3 d - \mathrm{sat}_\lambda(B^T P \hat{x})$; that is, for all $t \in [0, T]$,

$$\begin{aligned}|(x_2(t), x_3(t))| \leq \beta(|(x_2(0), x_3(0))|, t) \\ + \gamma\left(\sup_{t\in[0,T]} [-k_3 d(t) - \mathrm{sat}_\lambda(B^T P \hat{x}(t))]\right)\end{aligned} \tag{65}$$

where $\beta(\cdot,\cdot)$ is a class-$\mathcal{KL}$ function and $\gamma(\cdot)$ is a $\mathcal{K}$-class function. Since $\beta(\cdot, t)$ is a decreasing function in t and because $|d(t)| \leq |d(0)|$ and $|\mathrm{sat}_\lambda(B^T P \hat{x}(t))| \leq \lambda$, it follows from (65) that, in the interval $t \in [0, T]$, $|(x_2(t), x_3(t))|$ is bounded by a function of initial conditions that is independent of T. Likewise, using $\dot{x}_1 = x_2$ and (65), we conclude that $|x_1(t)|$ has an upper bound which is a continuous function of T, which contradicts the assumption $t_f < \infty$ because T can be arbitrarily close to t_f.

To prove stability of the equilibrium $(x, d) = 0$, we represent the closed-loop system (64) as in Proposition 1, where the x-subsystem is given by (30), and the z-subsystem is as in (32), with u replaced with $\tilde{u} = u - k_3 d$, and

$$w = g(z, u, d) = \begin{bmatrix} 0 \\ x_3|x_3| \\ -k_3 d \end{bmatrix} \tag{66}$$

in (31). Then, the same argument as in Theorem 2 implies that (37) holds for $\tilde{u} = u - k_3 d$ and, from $\|\tilde{u}\|_a \leq \max\{1, k_3\}(\|u\|_a + \|d\|_a)$, the gain condition (27) of Proposition 1 holds. Because $\|d\|_a = 0$, it follows from (29) that the equilibrium $(x, d) = 0$ is globally attractive. Finally, it is not difficult to show from the Jacobian linearization that the equilibrium is also stable. Having established stability and attractivity, we conclude that the equilibrium is globally asymptotically stable.

The proof of stability for the nested saturation design (38) is straightforward because the arguments in the proof of Proposition 2 continue to hold when x_3 is replaced with $\hat{x}_3 = x_3 + d$ where $\|d_a\| = 0$. ■

The proposed reduced-order observer takes as input the velocity in order to give an estimate of the flux signal ϕ. Since typical AMB sensors give position (as opposed to velocity) measurements, the required velocity signal has to be computed by differentiating the position. To avoid excessive noise in the observer input this may impose restrictions on the selection of the type and fidelity of position sensors used (i.e., optical instead of hall sensors, etc).

VIII. Numerical Examples

In this section we illustrate the previous theoretical results via a series of numerical simulations against a high-fidelity model of an one-dof AMB. The AMB model we consider has characteristics similar to those of Refs. [13], [17]. The AMB model in [13], [17] includes flux leakage, magnetic material saturation[3], flexible modes, voltage saturation and coil resistance. It has been shown that this mathematical model represents the actual AMB test rig very accurately, and hence it can be used to validate our control designs under realistic conditions [17]. Henceforth we call such a model the "actual" AMB model in order to distinguish it from the "ideal" model (with coil resistance, flux leakage, magnetic material saturation, flexible modes neglected) used for the control law design. The basic bearing properties are given in Table I. For more details of this AMB model one can consult Ref. [13] or [17]. Reference [17], in particular, has used this model to derive a high-performance voltage-driven controller for an one-dof AMB. The controllers were implemented to the actual AMB. The results of the simulations in [17] were essentially identical to the ones obtained via experiments, supporting the high-fidelity characterization of this AMB model.

TABLE I
AMB specifications

Symbol	Meaning
$N = 321$	♯ of turns in coil
$m = 4.5$ kg	effective mass of rotor
$\Phi_{\rm sat} = 200\ \mu$Wb	saturation flux
$A_g = 137$ mm^2	electromagnet pole area
$g_0 = 0.33$ mm (13 mils)	nominal width of airgap (when $x = 0$)
$V_{\max} = 10$ V	maximum voltage

The bias flux in all our simulations was chosen as $\Phi_0 = 10\ \mu$Wb. This corresponds to $\varepsilon = 0.1$ and it is an order of magnitude less than what is typically used in practice[4]. Also, the saturation level was chosen as $V_{\max} = 10$ V to make this specification a bit more challenging (the voltage saturation level in [13] and [17] is set to $V_{\max} = 30$ V). This voltage saturation level corresponds to $\lambda = 0.4$. Moreover, all control laws (specifically (31) and (22)) were implemented using their "hard" saturation counterparts.

[3]For simplicity, magnetic material saturation effects were neglected in the simulations. This was deemed acceptable because in all simulations the flux never exceeded 100 μWb, the value when magnetic saturation effects start becoming noticeable.

[4]A value of 40-50% of the saturation flux is used for most typical biasing schemes.

Two representative sets of numerical simulations are presented here. The initial conditions for all simulations were chosen as $q(0) = 0.15$ mm, $\dot{q}(0) = 0$ mm/sec, $\phi_1(0) = 10\ \mu$Wb and $\phi_2(0) = 50\ \mu$Wb. The initial condition for the auxiliary state ϕ is therefore $\phi(0) = -40\ \mu$Wb. This is significantly higher than one expects to encounter in practice (see second footnote on page 3) and it has been chosen to challenge the simplifying assumptions made during the control design. The initial state of the observer was always taken to be zero.

The first set of simulations demonstrates the effect of the observer gain κ. To this end, the ideal AMB model (no coil resistance, no flux leakage, etc) was used and the results are shown in Fig. 4. These plots show the results of the simulations with the control law (31) (state-feedback design) and three output feedback designs for three values of the observer gain κ. As shown in Fig. 4 the trajectories of the observer-controller interconnection tend to the trajectories of the state-feedback controller with increasing κ. Similar results hold for the control laws (22) and (38). At the bottom row of Fig. 4 the time histories of the auxiliary flux state ϕ and the control voltage V are shown. The actual flux and voltage command to each electromagnet are shown in Fig. 5. Notice, in particular, that the voltages V_1 and V_2 are applied to each electromagnet according to the sign of the auxiliary signal ϕ. The total fluxes Φ_1 and Φ_2 are given by $\Phi_1 = \Phi_0 + \phi$ and $\Phi_2 = \Phi_0 + \min\{\phi_1(0), \phi_2(0)\}$ when ϕ is positive and $\Phi_2 = \Phi_0 - \phi$ and $\Phi_1 = \Phi_0 + \min\{\phi_1(0), \phi_2(0)\}$ when ϕ is negative. This is implied by (6) and (8) and it is verified from the upper right plot of Fig. 5.

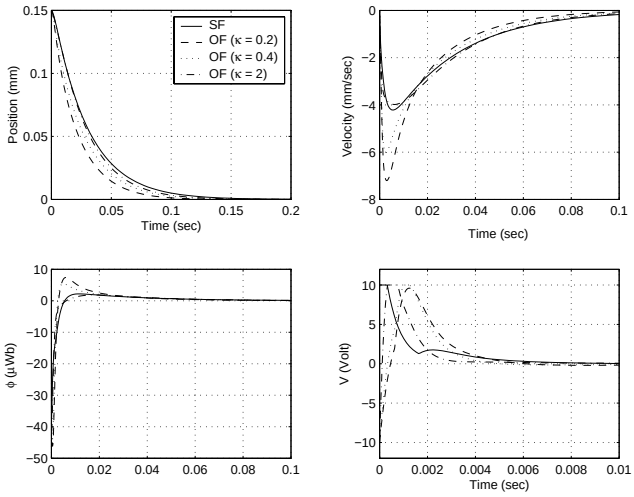

Fig. 4. State-feedback and output-feedback system trajectories with control law (31) and different observer gains. Controller gains $k_2 = k_3 = 5$.

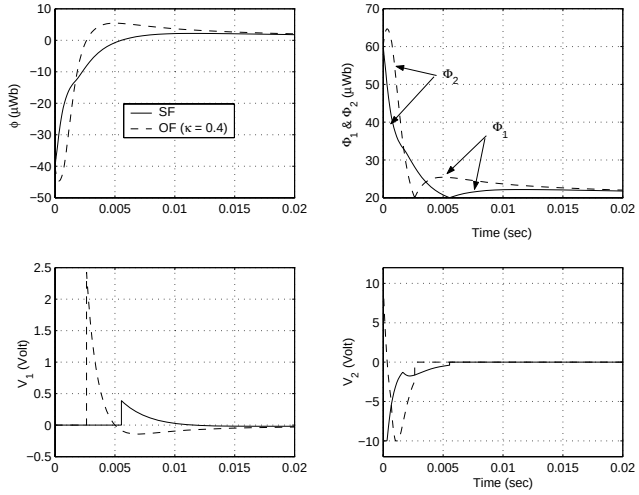

Fig. 5. State-feedback and output-feedback fluxes and command voltages with control law (31). Controller gains $k_2 = k_3 = 5$.

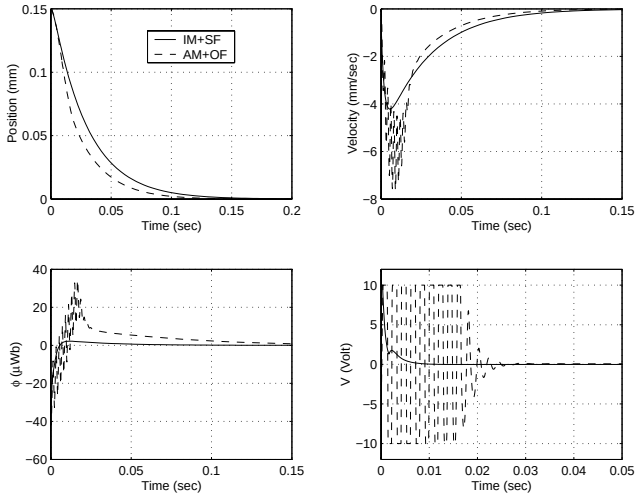

Fig. 7. Comparison of state trajectories and control inputs for ideal model (IM) with state feedback (SF) control law (22) and actual model (AM) with output-feedback (OF) implementation. Controller gains $k_1 = 20, k_2 = 2, k_3 = 1$. Observer gain $\kappa = 40$.

The second set of simulations compares the state trajectories and control signals of the ideal AMB plant with a state feedback control law, with the state trajectories and control signals of the actual (high-fidelity) AMB plant with the output feedback implementation of the same controller. The results for all three controllers are shown in Figs. 6-7. The initial conditions are the same as before. The observer gain for all the simulations was chosen as $\kappa = 40$. The results with controller (31) and controller gains $k_2 = k_3 = 5$ are shown in Fig. 6. The results with controller (22) and controller

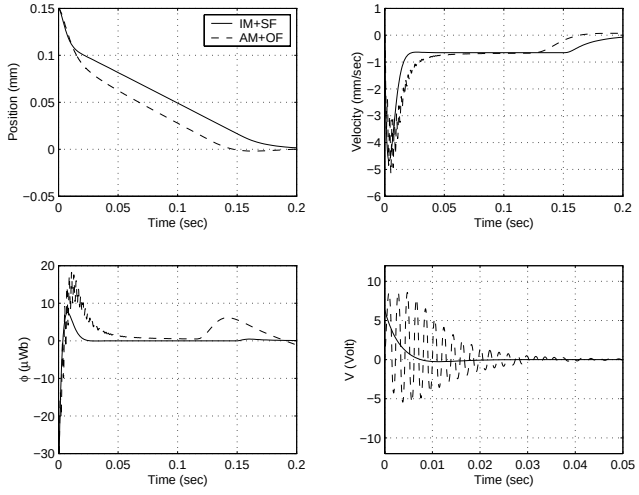

Fig. 6. Comparison of state trajectories and control inputs for ideal model (IM) with state feedback (SF) control law (31) and actual model (AM) with output-feedback (OF) implementation. Controller gains $k_2 = k_3 = 5$. Observer gain $\kappa = 40$.

gains $k_1 = 20, k_2 = 2, k_3 = 1$ are shown in Fig. 7. Finally, the simulation results with the saturated control law (38) are shown in Fig. 8. Since the saturation levels (39) are conservative, the values $\lambda_2 = \lambda_1/2$ and $\lambda_3 = \lambda_2/2$ (of course $\lambda_1 = \lambda = 0.4$) were used in these simulations to achieve faster system response. In

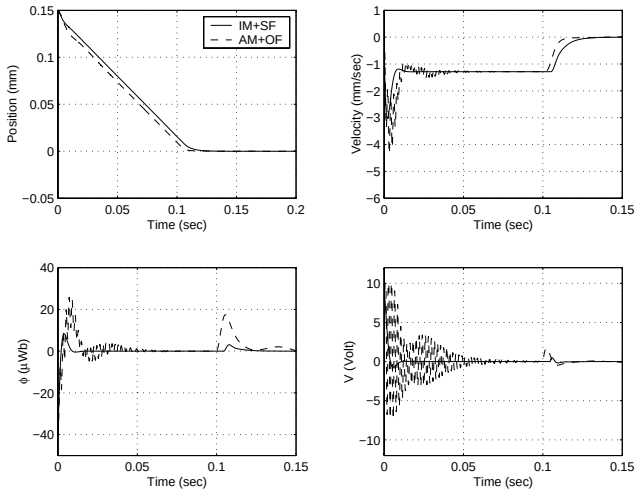

Fig. 8. Comparison of state trajectories and control inputs for ideal model (IM) with state feedback (SF) control law (38) and actual model (AM) with output-feedback (OF) implementation. Controller gains $k = 1, \lambda_2 = \lambda_{\max}/2, \lambda_3 = \lambda_{\max}/4$. Observer gain $\kappa = 40$.

all cases stability is achieved and the responses of the output feedback implementation on the actual bearing corroborate the state feedback responses predicted from the implementation on the ideal bearing model used for controller design. The highly oscillatory response of the output feedback implementation evident in these plots is due to the flexible modes. A closer examination of the results also showed that the neglected coil resistance was

the main factor contributing to the discrepancy between the ideal and actual model responses. If the resistance does not change significantly during the operation of the AMB, this term may be automatically compensated by most modern power amplifiers (see first footnote on page 3). In that respect, one expects the discrepancy between the ideal and actual responses to be smaller in practice.

IX. Conclusions

Low-bias operation of active magnetic bearings is essential for minimizing ohmic and eddy current losses. Due to the nonlinear nature of force vs. flux characteristic, operation at low-bias levels leads to reduced linear controllability and the use of high voltage commands. Low-bias control of an active magnetic bearing subject to voltage saturation can thus be a challenging control problem. In this paper we have presented three different designs for low-bias operation of active magnetic bearings using ideas from passivity, the asymptotic small-gain theorem of Teel, and nonlinear saturated control theory. A flux-based model for an active magnetic bearing that incorporates a generalized complementary flux condition is proposed and is used for control design. Since flux is not typically available for feedback we also propose a nonlinear reduced-order observer to estimate the flux from velocity measurements. We have shown that this flux observer, when interconnected in a certainty-equivalence implementation with the proposed state-feedback controllers, results in a globally asymptotically stable system.

Acknowledgments: The authors would like to thank Prof. A. Teel and Prof. E. Maslen as well the anonymous reviewers for their helpful comments. Support for the first author was provided by AFOSR (award no. F49620-00-1-0374) and NSF (award no. CMS-9996120).

References

[1] P. Allaire, M. Kasarda, and L. K. Fujita, "Rotor Power Losses in Planar Radial Magnetic Bearings - Effects of Number of Stator Poles, Air Gap Thickness, and Magnetic Flux Density," in *Proceedings of the 1998 International Gas Turbine and Aeroengine Congress and Exhibition*, 1998. Stockholm, Sweden.

[2] M. Arcak, and P. Kokotović, "Nonlinear observers: a circle criterion design and robustness analysis ," *Automatica*, Vol.37, No.12, 2001.

[3] M. D. Anderson and S. C. Dodd, "Battery Energy Storage Technologies," *International Journal of Control*, Vol. 81, No. 3, pp. 475–479, 1993.

[4] Anonymous, "Economic and Technical Feasibility Study for Energy Storage Flywheels," December 1983. Technical Report ERDA-76-65.

[5] J. C. Anselmo, "Technology Leaps Shape Satellites of Tomorrow," *Aviation Week and Space Technology*, pp. 56–58, January 25 1999.

[6] M. Baloh, G. Tao, and P. Allaire, "Modeling and Control of a Magnetic Bearing Actuated Beam," in *Proceedings of the American Control Conference*, pp. 1602–1606, 2000. Chicago, IL.

[7] A. Charara, J. De Miras, and B. Caron, "Nonlinear Control of a Magnetic Levitation System Without Premagetization," *IEEE Transactions on Control Systems Technology*, Vol. 4, No. 5, pp. 513–523, 1996.

[8] J. M. Coron, L. Praly, and A. Teel, "Feedback Stabilization of Nonlinear Systems: Sufficient Conditions and Lyapunov and Input-Output Techniques," in *Trends in Control: A European Perspective* (A. Isidori, ed.), pp. 293–348, London: Springer-Verlag, 1995.

[9] C. D. Hall, "High-Speed Flywheels for Integrated Energy Storage and Attitude Control," in *Proceedings of the American Control Conference*, pp. 1894–1898, 1997. Albuquerque, NM.

[10] D. Johnson, G. V. Brown, and D. J. Inman, "Adaptive Variable Bias Magnetic Bearing Control," in *American Control Conference*, (Philadelphia, PA), pp. 2217–2223, 1998.

[11] F. Keith, *Implicit Flux Feedback Control for Magnetic Bearings*, Ph.D. dissertation, University of Virginia, Charlottesville, Virginia, 1993.

[12] C. Knospe and C. Yang, "Gain-Scheduled Control of a Magnetic Bearing with Low Bias Flux," in *36th Conference on Decision and Control*, (San Diego, CA), pp. 418–423, 1997.

[13] C. Knospe, "The Nonlinear Control Benchmark Experiment," in *Proceedings of the American Control Conference*, pp. 2134–2138, 2000. Chicago, IL.

[14] M. Krstić, I. Kanellakopoulos, and P. Kokotović, *Nonlinear and Adaptive Control Design*, New York: Wiley and Sons, 1995.

[15] L. Li, "Linearizing Magnetic Bearing Actuators by Constant Current Sum, Constant Voltage Sum, and Constant Flux Sum," *IEEE Transactions on Magnetics*, Vol. 35, No. 1, pp. 528–535, 1999.

[16] Z. Lin and C. Knospe, "A Saturated High Gain Control for a Benchmark Experiment," in *Proceedings of the American Control Conference*, pp. 2644–2648, 2000. Chicago, IL.

[17] J. D. Lindlau and C. Knospe, "Feedback Linearization of an Active Magnetic Bearing with Voltage Control," *IEEE Transactions on Control Systems Technology*, Vol. 10, No. 1, pp. 21–31, 2002. To appear.

[18] W. Liu, Y. Chitour, and E. Sontag, "On Finite-Gain Stabilizability of Linear Systems Subject to Input Saturation," *SIAM Journal on Control and Optimization*, Vol. 34, No. 4, pp. 1190–1219, 1996.

[19] E. Maslen, P. Hermann, and M. Scott, "Practical limits to the performance of magnetic bearings: Peak force, slew rate and displacement sensitivity," *ASME Journal on Tribology*, vol. 111, pp. 331–336, 1989.

[20] E. Maslen, "Magnetic Bearings." Graduate Seminar Notes, Dept. of Mechanical and Aerospace Engineering, University of Virginia, June 2000.

[21] P. Proctor, "Flywheels Show Promise for 'High-Pulse' Satellites," *Aviation Week and Space Technology*, p. 67, January 25 1999.

[22] N. N. Rao, *Elements of Engineering Electromagnetics*, Englewood Cliffs, NJ: Prentice Hall, 4th ed., 1994.

[23] G. E. Rodriguez, P. A. Studer, and D. A. Baer, "Assessment of Flywheel Energy Storage for Spacecraft Power Systems," 1983. Technical Report TM-85061.

[24] R. Sepulchre, M. Janković, and P.V. Kokotović, *Constructive Nonlinear Control*, London: Springer-Verlag, 1997.

[25] E.D. Sontag, and Y. Wang, On Characterizations of the Input-to-State Stability Property. *Systems & Control Letters*, Vol. 24, pp. 351–359, 1995.

[26] J. R. Stuart and J. G. Stuart, "Revolutionary Next Generation

Satellite Communications Architectures and Systems," in *Proceedings of the 1997 IEEE Aerospace Conference*, pp. 535–545, 1997. Aspen, CO.

[27] H. Sussmann, E. D. Sontag, and Y. Yang, "A General Result on the Stabilization of Linear Systems Using Bounded Controls," *IEEE Transactions on Automatic Control*, Vol. 39, No. 12, pp. 2411–2425, 1994.

[28] A. Teel, "Using saturation to stabilize a class of single-input partially linear composite systems," in *Preprints of the 2nd IFAC Nonlinear Control Systems Design Symposium*, (Bordeaux, France), pp. 224–229, 1992.

[29] A. Teel, "A Nonlinear Small Gain Theorem for the Analysis of Control Systems with Saturation," *IEEE Transactions on Automatic Control*, Vol. 41, No. 9, pp. 1256–1270, 1996.

[30] P. Tsiotras, B. Wilson, and R. Bartlett, "Control of a Zero-Bias Magnetic Bearing Using Control Lyapunov Functions," *Proceedings of the 39th IEEE Conference on Decision and Control*, Sydney, Australia, pp. 4048–4053, 2000.

[31] P. Tsiotras and B. Wilson, "Zero- and Low-Bias Control Designs for Active Magnetic Bearings," *IEEE Transactions on Control Systems Technology*, 2003. to appear.